Environmental Science & Technology

Article

Cite This: Environ. Sci. Technol. 2019, 53, 4977−4987

pubs.acs.org/est

Bouncier Particles at Night: Biogenic Secondary Organic Aerosol Chemistry and Sulfate Drive Diel Variations in the Aerosol Phase in a Mixed Forest

Jonathan H. Slade,[*,†,$] Andrew P. Ault,[*,‡,§] Alexander T. Bui,[∥] Jenna C. Ditto,[⊥] Ziying Lei,[‡] Amy L. Bondy,[§] Nicole E. Olson,[§] Ryan D. Cook,[§] Sarah J. Desrochers,[†] Rebecca M. Harvey,[†] Matthew H. Erickson,[#] Henry W. Wallace,[∥] Sergio L. Alvarez,[#] James H. Flynn,[#] Brandon E. Boor,[∇] Giuseppe A. Petrucci,[○] Drew R. Gentner,[⊥] Robert J. Griffin,[∥,◆] and Paul B. Shepson[†,¶,▲,■]

[†]Department of Chemistry, Purdue University, West Lafayette, Indiana 47907, United States

[‡]Department of Environmental Health Sciences, University of Michigan, Ann Arbor, Michigan 48109, United States

[§]Department of Chemistry, University of Michigan, Ann Arbor, Michigan 48109, United States

[∥]Department of Civil and Environmental Engineering, Rice University, Houston, Texas 77005, United States

[⊥]Department of Chemical and Environmental Engineering, Yale University, New Haven, Connecticut 06520, United States

[#]Department of Earth and Atmospheric Sciences, University of Houston, Houston, Texas 77204, United States

[∇]Lyles School of Civil Engineering, Purdue University, West Lafayette, Indiana 47907, United States

[○]Department of Chemistry, University of Vermont, Burlington, Vermont 05405, United States

[◆]Department of Chemical and Biomolecular Engineering, Rice University, Houston, Texas 77005, United States

[¶]Department of Earth, Atmospheric and Planetary Sciences, Purdue University, West Lafayette, Indiana 47907, United States

[▲]Purdue Climate Change Research Center, Purdue University, West Lafayette, Indiana 47907, United States

Supporting Information

ABSTRACT: Aerosol phase state is critical for quantifying aerosol effects on climate and air quality. However, significant challenges remain in our ability to predict and quantify phase state during its evolution in the atmosphere. Herein, we demonstrate that aerosol phase (liquid, semisolid, solid) exhibits a diel cycle in a mixed forest environment, oscillating between a viscous, semisolid phase state at night and liquid phase state with phase separation during the day. The viscous nighttime particles existed despite higher relative humidity and were independently confirmed by bounce factor measurements and atomic force microscopy. High-resolution mass spectrometry shows the more viscous phase state at night is impacted by the formation of terpene-derived and higher molecular weight secondary organic aerosol (SOA) and smaller inorganic sulfate mass fractions. Larger daytime particulate sulfate mass fractions, as well as a predominance of lower molecular weight isoprene-derived SOA, lead to the liquid state of the daytime particles and phase separation after greater uptake of liquid water, despite the lower daytime relative humidity. The observed diel cycle of aerosol phase should provoke rethinking of the SOA atmospheric lifecycle, as it suggests diurnal variability in gas−particle partitioning and mixing time scales, which influence aerosol multiphase chemistry, lifetime, and climate impacts.

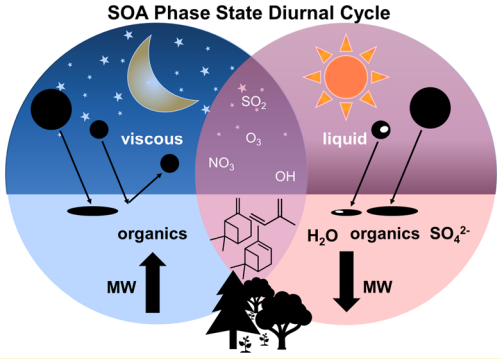

INTRODUCTION

Secondary organic aerosol (SOA), formed from both gas-phase oxidation and condensed-phase reactions involving anthropogenic and biogenic volatile organic compounds (BVOCs), constitutes a significant fraction of the global aerosol budget and the most abundant type of organic aerosol in the atmosphere.[1] SOA impacts climate directly by scattering or absorbing radiation and indirectly by altering the radiative properties of clouds and serving as ice nuclei.[2] However, there are order-of-magnitude differences in the global SOA burden according to atmospheric models, leading to significant uncertainties regarding SOA impacts on the radiative budget.[3]

The uncertainties associated with SOA impacts on climate result in part from limited knowledge of the chemical transformations and physical state of aerosol during its lifetime

Received: January 9, 2019
Revised: April 3, 2019
Accepted: April 19, 2019
Published: April 19, 2019

DOI: 10.1021/acs.est.8b07319
Environ. Sci. Technol. 2019, 53, 4977−4987

in the atmosphere.[4,5] While SOA has traditionally been assumed to be in a homogeneous liquid state, recent laboratory, field, and modeling studies have demonstrated that SOA formed from a variety of BVOC-oxidant systems and in different environments can exist as amorphous solids, semisolids, and phase-separated particles.[6−16] Shiraiwa et al.[13] used a model to predict that the phase state of particles varies spatially around the globe and with altitude depending on temperature, relative humidity, and particle composition (molar mass and characteristics such as the oxygen-to-carbon ratio of the organic matter, O/C) on an annual average. Such variations in particle phase state can significantly impact aerosol reactivity,[17−20] the long-range transport of toxic substances,[21,22] and the uptake and partitioning of semivolatile organic compounds and water vapor.[8,23−28] These processes affect the lifetime of SOA and its optical[29] and cloud condensation/ice nuclei activation properties.[30−33]

Field studies have aimed to characterize the phase state of atmospheric SOA particles based on the analysis of particle bounce factors (BF) in different forested environments, including the boreal forest region of northern Finland,[6] the Amazon rain forest of Brazil,[34] and a mixed deciduous/coniferous forest in the southeastern US.[12] While these studies together suggest phase state varies by location, with solid-like particles in the colder, monoterpene-dominated boreal forests, and liquid-like particles in the humid, isoprene-dominated forests of the Amazon, it has remained unclear if phase state changes over the diel cycle, despite the obvious contrasts in temperature, relative humidity, boundary layer height and atmospheric transport, light availability, and BVOC emissions.[35,36] For example, monoterpenes and the nitrate radical can become the dominant BVOC-oxidant system in forests at night, generating SOA with very different molecular properties and viscosity than that formed from daytime isoprene photooxidation.[13,16,23,28,37−39] Furthermore, the viscosity of SOA can be very sensitive to modulations in aerosol liquid water (ALW) content, which depend on the ambient relative humidity, water-soluble organic carbon content, and inorganic mass fraction.[9,10]

Herein, we analyze the ambient particle phase state over multiple daily cycles in a mixed deciduous/coniferous forest during the Atmospheric Measurements of Oxidants in Summer (AMOS) study in 2016 at the University of Michigan Biological Station (UMBS) PROPHET research site.[40] This work expands on prior BF field measurements by integrating high-frequency (1 Hz) day and night BF measurements with an electrical low-pressure impactor (ELPI) and single particle and bulk chemical composition, phase, and morphology analyses employing a suite of microscopy and high-resolution mass spectrometry instrumentation. Together, these measurements provided detailed quantitative information on the daily cycles of water-soluble ions, total organic mass, and other composition measures important when assessing compositional drivers of particle phase state, including average molar mass (M) and O/C ratios and estimates of ALW.

■ MATERIALS AND METHODS

Site Description and Field Study Timeline. The PROPHET-AMOS study was a large-scale field campaign conducted at the University of Michigan Biological Station in northern Michigan from July 1 to July 31, 2016. The measurements presented herein were made at the PROPHET tower research site (45°33′N, 84°42′W) underneath the mixed deciduous/coniferous forest canopy (canopy height ∼22 m) from July 9 to July 24. The PROPHET research tower is ∼5.5 km east of the town of Pellston, MI (population <800), and the nearest major metropolitan areas are Chicago, IL (472 km SW), Milwaukee, WI (375 km SW), and Detroit, MI (350 km SE). Other details of the site, including forest composition, BVOC emissions, and the impacts of different aerosol sources can be found in several previous studies.[40−42]

Meteorological and SO_2 Measurements. Meteorological measurements were conducted ∼6 m above the ground and were collocated with the trace gas sample inlets for the University of Houston Mobile Air Quality Laboratory (UHMAQL). Temperature and relative humidity were measured with a R. M. Young 41382 sensor, and pressure was measured with a R. M. Young 61302 V pressure sensor. SO_2 was measured using a pulsed fluorescence analyzer (Thermo Environmental, Inc.; model 43i-TL). Baseline determinations were made once per hour by flowing ambient air over a carbonate-treated filter to selectively remove SO_2 from the sample. Instrument sensitivity was established by daily challenges with zero-air dilutions of a NIST-traceable gas standard (Scott-Marrin, Inc., Riverside, CA).

Electrical Low-Pressure Impactor Sampling. Two electrical low pressure impactors (ELPIs; Dekati ELPI+ and High Resolution-ELPI+[43]) housed in the University of Michigan Mobile Laboratory were employed to determine particle bounce factors (BFs).[44] One ELPI was operated with sintered substrates[45] and the other with smooth aluminum foil substrates. The two ELPIs sampled particles simultaneously at a rate of 10 L min^{-1} through ∼2 m long 1/2″ ID insulated copper tubing connected to a 12″ L × 4″ ID cylindrical sampling manifold, which was adapted to a ∼3 m long 1″ ID stainless steel tube oriented vertically on top of the trailer roof. There were no differences in the relative humidity or temperature measured outside and at the base of the ELPI in the lab during sampling. The ELPIs sampled particles with an aerodynamic diameter between 0.006 to 10 μm across 14 electrically detected stages at a rate of 1 Hz. The BF data presented in this work are 10 min averages of the 1 Hz BF data. It is important to note that BF is used in this study to infer changes to particle phase state on relatively shorter time scales than is allowable by offline analysis, and should be regarded as a mechanical property, dependent on both the chemical and physical properties of the particles as well as the surface characteristics and flow dynamics in the impactor.[46] Further details regarding the BF calculation can be found in the SI.

High-Resolution Time-of-Flight Aerosol Mass Spectrometry. A high-resolution time-of-flight aerosol mass spectrometer (HR-ToF-AMS, Aerodyne Research Inc.) was used to measure nonrefractory submicron aerosols.[47] In brief, particles were sampled through a 100 μm critical orifice and were focused into a particle beam using an aerodynamic lens. After traversing a vacuum chamber, the particles in the beam were impacted onto a tungsten vaporizer heated to 600 °C. Vapors were subsequently ionized by electron impact ionization (70 eV). The HR-ToF-AMS was operated in a high mass sensitivity mode, referred to as V-mode. The sampling inlet for the HR-ToF-AMS measurement was collocated with the UHMAQL meteorological measurements. The inlet was fitted with a $PM_{2.5}$ cyclone. Further details of ionization efficiency calibrations, data analysis, and ALW determination by ISORROPIA can be accessed in the SI.

DOI: 10.1021/acs.est.8b07319
Environ. Sci. Technol. 2019, 53, 4977−4987

Particle Collection by MOUDI and Analysis by Atomic Force Microscopy. Particle samples for atomic force microscopy (AFM) were collected using a micro-orifice uniform deposition impactor (MOUDI, model 110, MSP Corp.) and collocated with the ELPI. Particles were sampled from 5.5 m above ground level through an insulated 1.1 cm inner diameter copper tubing inlet using a cylindrical sampling manifold. Particles were impacted on silicon wafers (Ted Pella Inc.) on stages 5, 7, 9, and the backup filter of the MOUDI, and samples from July 10, 2016 (day) and July 16, 2016 (night) on stage 9 of the MOUDI were analyzed at the University of Michigan. AFM analysis at ambient temperature and pressure was initially performed on a NanoIR2 system (Anasys Instruments) followed by analysis with a PicoPlus 5500 AFM (Agilent) after rehumidification to 80% RH where they equilibrated prior to analysis at 50% RH (similar RH values to ambient collection conditions). SEM-EDX analysis was used to confirm that the particles analyzed were primarily organic carbon or organic-sulfate mixtures. Particles <180 nm (stage 9) were primarily organic and sulfate, with EDX showing C, O, S, and N as the predominant elements, which prior work at UMBS has shown is organic material and sulfate.[42,48−50] Less than 3% of daytime particles and 1% of nighttime particles contained markers for salts (other than ammonium sulfate) and dust (Na, Mg, K, Ca, P, Al, and Cl), though these are observed in larger particles at the site.[49,51] Further details of the AFM and SEM-EDX analysis can be found in the SI.

High-Performance Liquid Chromatography Electrospray Ionization Time-of-Flight Tandem Mass Spectrometry. A custom-built sampler was positioned on the PROPHET tower 28 m above the ground, facing west. Samples were collected on PTFE membrane filters (47 mm diameter, 1.0 μm pores, Tisch Environmental) housed in passivated stainless-steel filter holders (Pall Corporation). No upstream inlet tubing was used to minimize potential aerosol loss to tubing walls. Samples were collected at 1 m^3 hr^{-1} for maximum collection efficiency. An 84-mesh stainless steel screen (McMaster Carr) was installed over the inlet that prevented large particles and insects from contaminating the filters and limited particle size to approximately PM_{10} at a flow rate of 1 m^3 hr^{-1}. Samples were collected both during the day (9:00 am−5:00 pm) and at night (9:30 pm−5:30 am), avoiding sunrise and sunset, to capture products of daytime and nighttime oxidation chemistry without the influence of transitional chemistry during dawn and dusk. Field blanks were collected alongside all samples in identical holders. Filters were sonicated and extracted in methanol, and the extracts were frozen immediately and then thawed prior to analysis. The extracts were analyzed with an Agilent 1260 Infinity HPLC with an Agilent 6550 Q-TOF mass spectrometer, using an electrospray ionization (ESI) interface. We note that some fraction of the carboxylic acids and carbonyl compounds in the filter samples may have been converted to esters and (hemi)acetals, respectively, during extraction in methanol.[52] If conversion in the frozen methanol extracts occurred, this implied that the O/C ratios and viscosity we reported in this study could be slightly underestimated. Further details can be found in the SI.

RESULTS AND DISCUSSION

Diel Patterns and the Impact of Mixing State, Size, and Liquid Water on Particle Bounce. Figure 1 shows the composite median diel trend in BF from the individual daily BF profiles presented in Figure S1. BF exhibits a maximum in the early morning (between 03:00 and 06:00 EDT), decreasing following sunrise to a minimum during the day (between 12:00 and 14:00 EDT) and then increasing into and through the late evening. For comparison, the median BF values are similar in range to those measured in a mixed forest in the southeastern U.S.,[12] indicating that the particles are characteristic of semisolids but transition to lower viscosity particles during the day.[9,12,44]

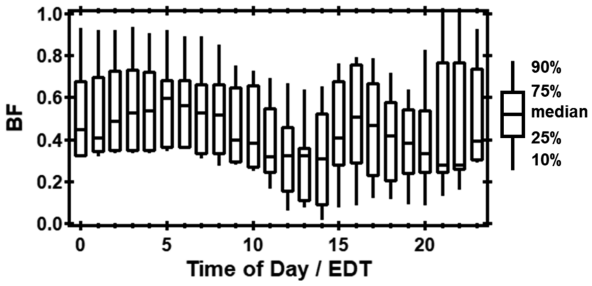

Figure 1. Diel trend in BF showing median and percentiles for each hour corresponding to all BF measurement periods in this study.

Single particle analysis[53] confirmed that BF reflects particle phase state by contrasting BF with the morphology and phase of the particles using atomic force microscopy (AFM)[54] at ambient pressure and RH, with corroboration from scanning electron microscopy (SEM).[28] Figure 2 shows representative AFM height and phase images of particles impacted onto silicon wafers using a micro-orifice uniform deposit impactor (MOUDI) (0.10−0.18 μm) during a low BF period (ranging between ∼0.2 and ∼0.3) during the day and a high BF period (ranging between ∼0.6 and ∼0.8) at night. Because particle size is an important parameter impacting phase transitions,[55] phase separation,[56] and bounce,[7,11] though highly uncertain,[57] we examined the impact of particle size on the phase state by determining how the spreading ratios (ratio of radius to height, where 1 is a hemisphere) of particles with volume equivalent diameters <100 nm and >100 nm differ between night and day. This analysis was conducted both as collected and after rehumidifying the samples to 80% RH followed by analysis at 50% RH, to reproduce ambient RH. The spreading ratios in Figure 2e indicate less spreading for the higher BF particles <100 nm at night, which is indicative of more viscous particles,[54] confirming the lower spreading at night was representative of ambient conditions. In contrast, greater spreading was observed for the daytime samples <100 nm, which is in line with low BF observed during the day. AFM phase images of the daytime samples with more spreading also showed separate aqueous ammonium sulfate and organic phases, as has been shown previously with AFM.[58] Greater sulfur in the daytime particles was confirmed using SEM with energy dispersive X-ray spectroscopy (EDX), which is primarily sulfate based on prior measurements at UMBS.[50] We found that daytime and nighttime particles >100 nm have similar, high spreading ratios (12−13), indicative of aged, mixed inorganic, and organic accumulation mode particles with high water content. Thus, our results indicate that the observed diel cycle in BF is driven by the properties of relatively newly formed (<100 nm) particles, which prior measurements at UMBS suggest are of a local biogenic origin.[41,50]

HR-ToF-AMS further reveals that the bouncier particles at night contained a greater fraction of organic matter (f_{Org}) and

DOI: 10.1021/acs.est.8b07319
Environ. Sci. Technol. 2019, 53, 4977−4987

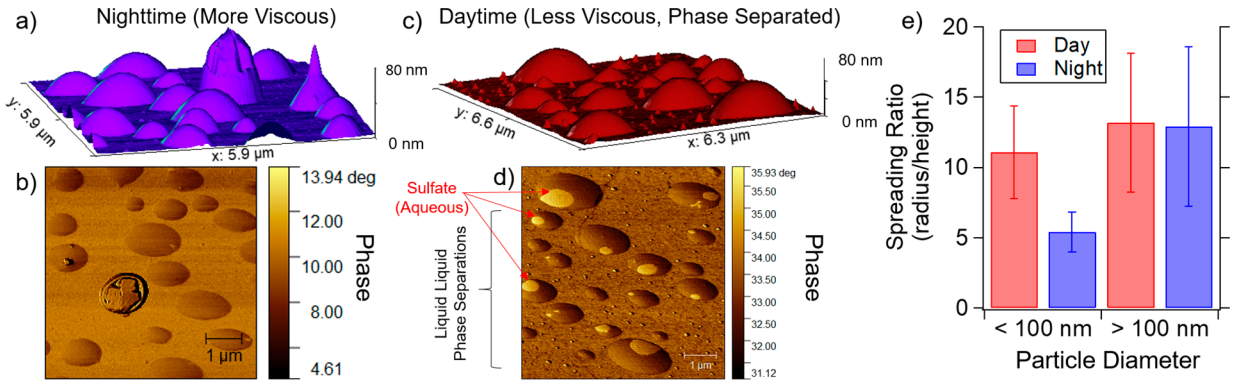

Figure 2. (a and c) AFM height images of taller (more viscous) nighttime particles (0.6 ≤ BF ≤ 0.8) and flatter daytime particles (0.2 ≤ BF ≤ 0.3). (b and d) AFM phase images of the same samples, with liquid−liquid phase separations indicated in the daytime sample. (e) Quantified spreading ratios for nighttime and daytime samples for particles <100 nm and >100 nm, where particles <100 nm at night exhibit less spreading than larger particles or daytime particles.

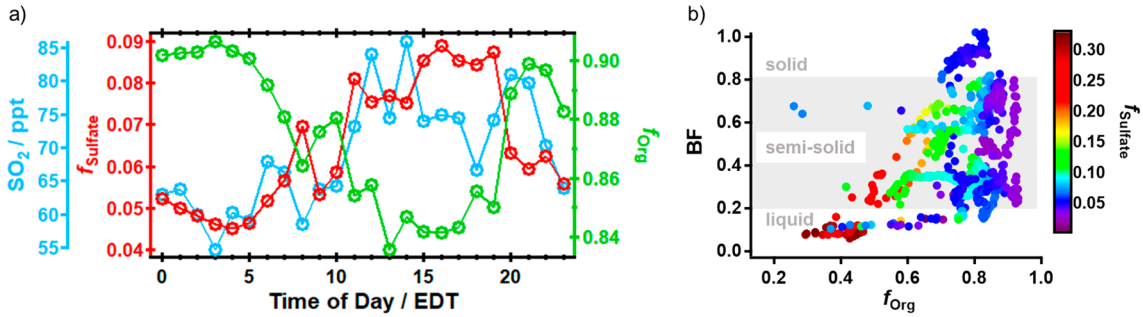

Figure 3. (a) Median diel SO_2, particulate sulfate mass fraction ($f_{Sulfate}$), and particulate organic matter mass fraction (f_{Org}). (b) BF as a function of f_{Org} and $f_{Sulfate}$ (shown in color scale). The gray shaded region in part b shows approximate cutoffs for the different phase state regimes. Below BF ∼ 0.2, particles are likely in a liquid-like state, in a transition or semisolid regime between 0.2 and 0.8, and highly viscous semisolids/solids above BF ∼ 0.8.

smaller fraction of particulate sulfate ($f_{Sulfate}$), compared to the daytime particles as shown in Figure 3a. There is an estimated minor contribution (<2%) from organosulfates based on the concentration of CS ion families in the mass spectra for both day and night aerosol, independently confirming the results from Figure 2, which is supported by a lack of Raman organosulfate modes[59] from previous measurements at UMBS.[48] According to Figure S2, the consistently higher $f_{Sulfate}$ during the day is likely driven by a shift in wind direction to more polluted regions from the south (HYSPLIT back trajectories[60] for each day are shown in Figure S3). VanReken et al.[42] characterized air masses impacting the PROPHET site from the south as having relatively higher concentrations of SO_2, sulfate, and water-soluble organic carbon (WSOC) with higher cloud condensation nuclei (CCN) activity than the mostly organic particles observed when flow is from cleaner regions to the north or west. In contrast, the shift to lighter and more westerly flow at night indicates that the nighttime aerosol was impacted more by local biogenic sources,[42] leading to the relatively higher f_{Org} at night. In addition, due to the shallower boundary layer, the more stagnant air at night can trap BVOC emissions (primarily terpenes due to lower isoprene emissions), their oxidation products, and aerosol particles near the surface, promoting condensational growth of organic matter on the particles and increase in f_{Org} at night.

The increase in sulfate and SO_2 during the day is expected to increase particle hygroscopicity, promoting water uptake and liquification of the particles.[9,10] Figure 3b shows the dependence of BF on f_{Org} and $f_{Sulfate}$ (color scale). In general, BF decreased with decreasing f_{Org} and increasing $f_{Sulfate}$, and notably, when f_{Org} ∼ 0.4, corresponding to $f_{Sulfate}$ ∼ 0.3, the BF < 0.2 indicates that the particles were primarily in a liquid-like state. Similar behavior in particle bounce has been noted for pure glucose particles exposed to H_2SO_4 and laboratory-generated biogenic SOA exposed to SO_2, where even minor enhancements in $f_{Sulfate}$ can lead to a significant loss of particle bounce.[6,9,10] Moreover, according to particle rebound fractions measured in Beijing, Liu et al.[61] showed that submicron aerosol particles are in a liquid state during urban haze episodes, which the authors attribute to significant enhancements in the water-soluble inorganic fraction and subsequent increase in ALW. However, this contrasts a recent study by Bateman et al.,[62] who observed an increase in BF more often at night associated with anthropogenic activity in the Amazon. Similarly, Vaden et al.[63] and Zelenyuk et al.[64] indicate that polycyclic aromatic hydrocarbon (PAH) emissions from combustion sources can increase viscosity and decrease SOA volatility. Figure S4 shows that potential PAH concentrations in our aerosol filter samples were indistinguishable between day and night, emphasizing the importance of sulfate and other biogenic components in controlling aerosol phase over the diel cycle. A subtle, but important, distinction to be made from Figure 3b is that although BF generally decreased with increasing $f_{Sulfate}$, the particles can remain in a liquid-like state (BF < 0.2) even at very low $f_{Sulfate}$ < 0.1. This suggests $f_{Sulfate}$ is not the only driver of BF but it is likely that other factors, e.g., the organic molecular composition of the aerosol, play an important role too.

DOI: 10.1021/acs.est.8b07319
Environ. Sci. Technol. 2019, 53, 4977−4987

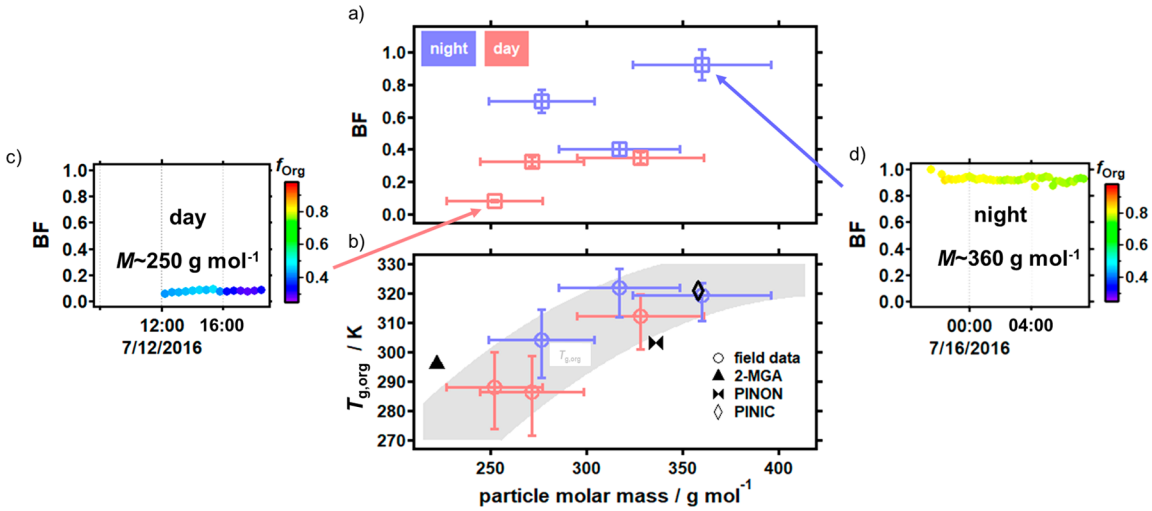

Figure 4. (a) BF (squares) and (b) $T_{g,org}$ (circles) as a function of M, where nighttime samples are in blue and daytime samples in red. The gray shaded region in part b shows the calculated range of $T_{g,org}$ bounded by O/C = 0.25 and O/C = 0.75. The black symbols represent the $T_{g,org}$ of common biogenic SOA dimers of pinic acid (PINIC, diamond), pinonaldehyde (PINON, bow tie), and 2-methylglyceric acid (2-MGA, triangle). The vertical error bars in BF (part a) represent 10% variability in the measured BF over the filter sampling period. M is weighted by LC peak abundances and shown with an uncertainty of 10% as discussed in detail in the Methods. The vertical error bars (part b) in dry $T_{g,org}$ account for the applied 10% uncertainty in M. (c and d) Example day and night BF time series, respectively, colored by AMS-derived organic mass fractions (f_{Org}).

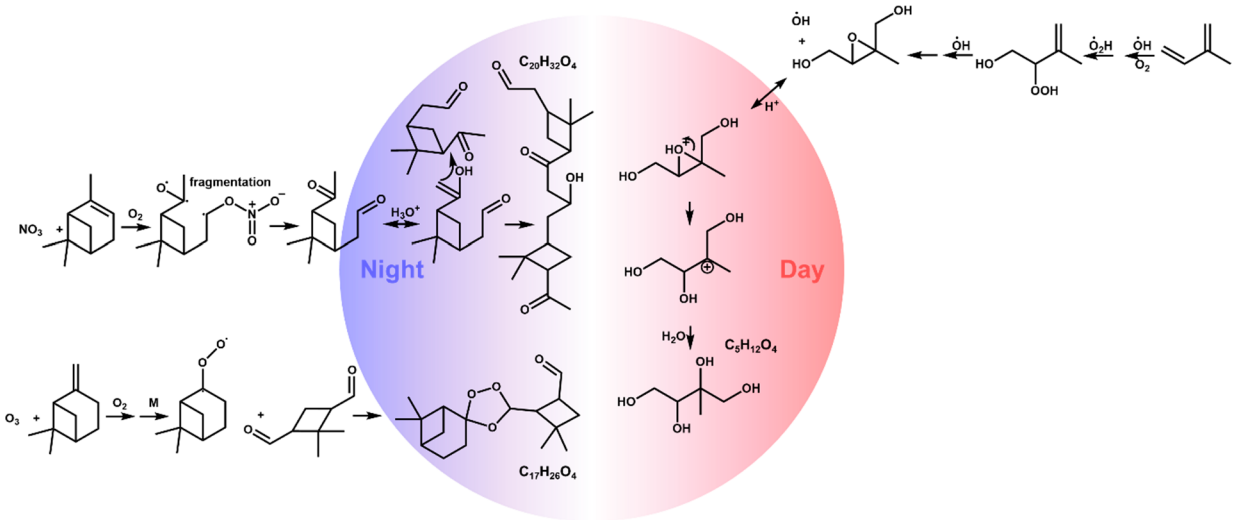

Figure 5. Relevant nighttime (blue) and daytime (red) BVOC oxidation and multiphase chemistry. Acid-catalyzed aldol condensation of pinonaldehyde and formation of product $C_{20}H_{32}O_4$ was adapted from Tolocka et al.[68] Formation of a secondary ozonide from β-pinene ozonolysis and formation of product $C_{17}H_{26}O_4$ was adapted from Heaton et al.[69] Relevant isoprene daytime chemistry leading to formation of 2-methyl-tetrol ($C_5H_{12}O_4$) was adapted from Surratt et al.[67]

Glass Transition Temperatures and the Role of Biogenic Emissions and Aerosol Liquid Water. Due to the large fraction of organic matter in the aerosol (81% by mass on a campaign average), we examine how the BF changes in response to the average molar mass (M) and O/C of particle-phase organic components. M and O/C express the degree of intermolecular bonding and are used here to determine particle glass transition temperatures (T_g) of the organic components, defined as the characteristic temperature for which a nonequilibrium phase transition occurs from a glassy solid state to a semisolid state as temperature increases.[8,13,16] This provides a link between BF, a mechanical property, and molecular composition. Equations for calculating BF[44] and T_g[13] can be found in the SI, eqs S1−S3. We calculated the M and O/C of aerosol particles collected using a high-volume PM10 filter sampler based on weighted average peak spectral intensities and assigned chemical formulas from HPLC-ESI-ToF-MS spectra in negative ion mode, as done previously.[65,66] Differences between the phase states of night and day aerosol were determined from the analysis of filter samples acquired in parallel with BF measurements over three 8 h daytime (7/12, 7/22, and 7/23) and nighttime sampling periods (7/15−7/16, 7/16−7/17, and 7/22−7/23). Figure 4a shows the average BF and Figure 4b shows the corresponding T_g of the dry organic components ($T_{g,org}$) as a function of M for the six independent collection periods. Example daytime and nighttime BF time series during filter collection are shown

DOI: 10.1021/acs.est.8b07319
Environ. Sci. Technol. 2019, 53, 4977−4987

in Figure 4c,d, respectively, and indicate little variability. Corresponding mass spectra are presented in Figure S5.

Figure 4 shows that the increase in the observed BF from ∼0.1 to ∼0.9 corresponds very well with the increase in M from ∼250 to ∼360 g mol^{-1}, leading to the ∼30 K increase in $T_{g,org}$. This indicates that the molecular composition of the organic components in the particles potentially contributes to differences in both phase state and bounce characteristics in the impactor. However, note the lower M periods also correspond to lower f_{Org}. For reference, estimated $T_{g,org}$ and corresponding M are in agreement with that of common biogenic SOA markers (2-MGA, lower M) and monoterpene-derived SOA (PINON and PINIC, higher M). Notably, $T_{g,org}$ was relatively higher at night on average, consistent with the higher BF measured at night. Detailed molecular composition analysis in Figure S6 confirmed that larger M oligomers related to monoterpene oxidation (C_{17} and C_{20} compounds) comprised a greater proportion of the nighttime particle mass, while smaller M compounds associated with isoprene SOA, including 2-methyltetrols ($C_5H_{12}O_4$) and an oligoester monomer ($C_5H_8O_5$),[39,67] constituted a greater fraction of the daytime particle mass. Figure 5 shows potential oligomer formation pathways from pinic acid and pinonaldehyde, formed from the oxidation of α- and β-pinene by O_3 and NO_3, and daytime relevant production of 2-methyl-tetrols from isoprene photooxidation by OH.

Table S1 shows the relative VOC reactivities of isoprene to monoterpenes for day and night assuming OH and O_3 are the dominant oxidants, and indicates that isoprene dominates daytime VOC reactivity, whereas monoterpenes dominate the VOC reactivity at night. This is important for understanding the contribution of BVOC oxidation chemistry to aerosol phase state, as several studies indicate that the aerosol composition and phase can be very different for isoprene and monoterpene SOA and depend on the specific BVOC-oxidant system. The NO_3 oxidation of terpenes produces relatively larger M oligomerization products[37] and highly viscous (higher $T_{g,org}$) aerosol[23] compared to isoprene photooxidation SOA, wherein monoterpene- and sesquiterpene-derived SOA, which are more relevant than isoprene SOA at night, remain highly viscous even under high, nighttime relevant, RH.[8,13,16,38] In contrast, daytime isoprene oxidation produces smaller M products, including isoprene epoxydiols (IEPOX) and 2-methyl-tetrols, which were in greater abundance in the daytime filter samples and are known to partition to and suppress the surface tension of aqueous SOA.[70] Such compounds could contribute to the relatively lower BF and T_g of the daytime particles. Moreover, aerosol phase OH oxidation[12] and photodegradation reactions during the day can create fragmented and volatile aerosol oxidation products,[71,72] thus reducing M, whereas NO_3 heterogeneous oxidation at night is not expected to increase aerosol volatility.[73] This suggests the oligomers formed at night are also susceptible to photodegradation during the day, triggering a positive feedback loop during the day whereby the decrease in particle viscosity promotes more uptake of pollutants, such as SO_2, which react to form inorganic ions in the particles, further decreasing particle viscosity.

To estimate the impact of ALW on the aerosol phase diel cycle, Figure 6 shows the predicted night and day ratios of T_g/T after correcting the average night and day $T_{g,org}$ for estimated ALW content, where T_g/T relates to viscosity (η) following the parametrization outlined in Shiraiwa et al.[13] and DeRieux et al.[16] Here, ALW was estimated from thermodynamic principles employing the ISORROPIA model for inorganic ions and Gordon−Taylor approximation for organics ascribing a hygroscopicity parameter (κ),[74,75] as discussed in the Supporting Information and eq S3. Although κ of the organic components is uncertain, prior work at UMBS measured relatively larger κ during periods of anthropogenic influence, as observed here during the day, and relatively smaller κ during periods of biogenic influence, as observed here at night.[42] Further, laboratory studies have shown that κ of terpene-derived SOA at equivalent nighttime RH (median diel cycles of RH and T are provided in Figure S7) is several times lower (κ ∼ 0.02 at 80% RH) compared to isoprene-derived SOA under relevant daytime RH (κ ∼ 0.15 at 60% RH).[38] Because we observed a distinct presence and greater abundance of monoterpene-derived SOA at night and isoprene-derived SOA during the day, we extend our analysis to κ_{org} = 0.15 during the day (09:00−20:00) and κ_{org} = 0.02 at night (21:00−08:00). These values are within the uncertainty in κ reported by VanReken et al.[42] for aerosol particles at UMBS assuming the inorganic fraction is primarily ammonium sulfate (κ_{inorg} = 0.63),[74] as confirmed for these measurements in Figure S8. Our analysis in Figure 6, while sensitive to the applied κ_{org} (see Figure S9), shows that η may be several orders of magnitude larger at night (up to ∼10^6 Pa·s) compared to that during the day (∼10^1 Pa·s), despite the higher RH at night, with the estimated daytime and nighttime η in the range of that measured previously for isoprene- and monoterpene-derived SOA, respectively.[16,76] Note that the abrupt night−day transition in Figure 6 is expected to be more gradual and is a consequence of fixing κ_{org} over two coarse 12 h daytime and nighttime sampling regimes, corresponding to the time frame of aerosol collection onto the filters. Notably, for all reasonable κ_{org} values applied, our analysis indicates that the daytime particles at this site are predictably in a liquid state ($\eta < 10^2$ Pa·s), and nighttime η is in the range of semisolids and highly viscous liquids ($10^2 < \eta \leq 10^6$ Pa·s), consistent with the diel cycle in BF.

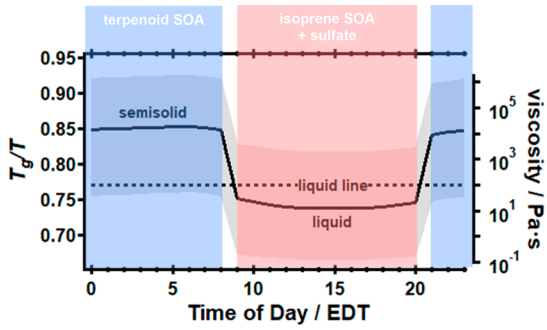

Figure 6. Diel trend in the estimated ratio of glass transition temperature to ambient T (T_g/T) and corresponding viscosity (η) corrected for inorganic- and organic-derived ALW, where the gray shaded area represents the upper and lower bounds of η assuming a fragility parameter of 20 and 5, respectively.[13] In this analysis, κ_{org} = 0.15 during the day (09:00−20:00) and κ_{org} = 0.02 at night (21:00−08:00). The liquid line ($\eta = 10^2$ Pa·s) represents the semisolid−liquid phase transition.[13,16]

The results presented in this study suggest different partitioning behavior of particle-phase components[24] and heterogeneous reactivity[19] at night and during the day, i.e. partitioning more readily with the particle bulk during the day and more with the particle surface at night. To test this, we

DOI: 10.1021/acs.est.8b07319
Environ. Sci. Technol. 2019, 53, 4977−4987

calculate the effect estimated nighttime and daytime η has on the characteristic equilibrium time scale for bulk diffusion (τ_{bd}) in a particle with diameter (d_p) according to $\tau_{bd} = \frac{d_p^2}{4\pi^2 D_b}$ where D_b is the molecular diffusion coefficient in the bulk derived from the Stokes−Einstein equation assuming a molecular radius of 1 nm.[8,13] Given the uncertainty in κ_{org} and the existence of multiple aerosol phases as shown in Figure 2, we show τ_{bd} over a range of predicted viscosities in Figure 7. Here,

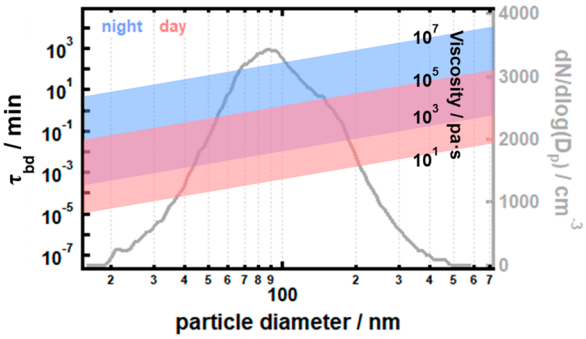

Figure 7. Estimated range in bulk diffusion times (τ_{bd}) and viscosity of night (blue) and day (red) aerosol sampled during this study as a function of particle diameter. Upper bounds in the estimated night and day τ_{bd} represent the τ_{bd} of phase-separated particles and lower bounds represent well-mixed inorganic/organic particles, as discussed in the text. The median particle size distribution measured by the SMPS during this study is shown in gray.

we assume the particles are either well-mixed or phase-separated. In the well-mixed case, the ALW effect on T_g includes combined ALW content from both the inorganic and organic matter (this yields the lower bound in τ_{bd}). In the phase-separated case, the ALW effect on T_g is considered isolated to either the organic or inorganic components (yielding the upper bound of τ_{bd}). A sensitivity analysis in Figure S10 shows how τ_{bd} changes with different κ_{org}. Also note that the Stokes−Einstein relation may underestimate bulk diffusivity in highly viscous matrices at temperatures near the glass transition.[15] As a result, although nighttime T_g/T was ∼0.85, it is possible our estimated nighttime τ_{bd} may be shorter than shown in Figure 7.

From Figure 7, nighttime aerosol exhibits relatively longer bulk diffusion time scales, increasing with diameter and degree of phase separation and decreasing as the inorganic and organic components become well mixed, i.e., with more ALW interaction with the organic matter. Estimated bulk diffusion time scales for particles between 50 and 300 nm (i.e., bulk of the observed size distribution) are shown to range from up to half an hour to several hours at night, whereas time scales are limited to under 20 min during the day. However, as we did not observe a significant difference in the spreading ratios of particles >100 nm in diameter in Figure 2e, we expect that the particles most impacted by day and night differences in bulk diffusion times are those <100 nm, where the estimated time scales range from <2 min during the day and up to 2 h at night. This result implies slower aerosol partitioning of semivolatile organic compounds, and thus potentially diffusion-limited particle mass growth at night.[23,24] Indeed, recent work shows that isoprene epoxide (IEPOX) uptake by acidified ammonium sulfate can be twice as slow when the particle is coated with α-pinene SOA,[28] suggesting that such reactions could affect the growth and chemical transformations of aerosol particles at night. Compounds in the particle phase may be relatively longer-lived overnight due to slower diffusion of reactants into the particle bulk and from the bulk to the surface,[17,19] contributing to the long-range transport of toxic pollutants embedded in the particles.[21,22] In addition, because of much greater surface uptake resistance for bouncier particles, the particles themselves are potentially longer lived at night with respect to dry depositional loss.[77] Given the clear differences in the phase states of monoterpene- and isoprene-derived SOA observed here and in other studies, our results also suggest that the current forest succession occurring at UMBS,[78] i.e., transition from predominately isoprene-emitting (deciduous) to predominately terpene-emitting forests (coniferous), could impact the physical nature of atmospheric SOA by altering the pool of reactive BVOCs and thus BVOC oxidation products, in general. It is important to note that the mixing state of different particle populations from differences in day-to-night transport dynamics can influence the phase state of the particles sampled in this study.[50] Particle mass loading[79] and air mass history may also influence particle phase state, as the time scale for water diffusion in viscous aerosol and the phase and morphology of particles depend on its atmospheric conditioning history (number of drying and humidification cycles, and drying rate).[80,81] Moreover, it is unclear how the diel behavior in aerosol phase and viscosity in this study compare to other forested and urban regions as it depends on the ambient temperature, relative humidity, composition of the reactive VOCs, and the extent of anthropogenic influence, e.g., mass of sulfate in the particles. In the boreal region, where conifers and monoterpene emissions dominate, or in regions such as the Amazon, where deciduous forests and isoprene emissions dominate, the diel cycle in aerosol phase may be unlike our observations, whereas the phase state of aerosol in mixed forest regions such as in the southeastern United States may exhibit a similar diel cycle. Therefore, it is critical that future research expand on these findings, through devoted field measurements in different environments and through atmospheric modeling, to help better constrain the impact of particle phase state diel variability on climate, air quality, and public health.

■ ASSOCIATED CONTENT

Supporting Information

The Supporting Information is available free of charge on the ACS Publications website at DOI: 10.1021/acs.est.8b07319.

HR-ToF-AMS ionization efficiency calibration and ALW determination by ISORROPIA; bounce factor calculation; filter extraction and analysis by HPLC-ESI-ToF-MS; glass transition temperature derivation; daytime and nighttime differences in isoprene- and monoterpene-derived SOA precursors; VOC reactivity table; BF daily time profiles; figures for diel wind direction and wind speed, relative humidity, and temperature; HYSPLIT back trajectories, double bond equivalence, and aromaticity index; night and day mass spectra from HPLC-ESI-ToF-MS; mole ratio of ammonium to sulfate; hygroscopicity effect on viscosity with time of day; and bulk diffusion time scales. (PDF)

■ AUTHOR INFORMATION

Corresponding Authors

*E-mail: jhslade@ucsd.edu.

DOI: 10.1021/acs.est.8b07319
Environ. Sci. Technol. 2019, 53, 4977−4987

*E-mail: aulta@umich.edu.

ORCID

Jonathan H. Slade: 0000-0002-5026-4229
Andrew P. Ault: 0000-0002-7313-8559
Nicole E. Olson: 0000-0003-1600-8050
Brandon E. Boor: 0000-0003-1011-4100
Giuseppe A. Petrucci: 0000-0002-1241-6674
Drew R. Gentner: 0000-0003-3066-2614

Present Addresses

[$]Department of Chemistry and Biochemistry, University of California San Diego, La Jolla, CA 92093
[■]School of Marine and Atmospheric Sciences, Stony Brook University, Stony Brook, NY 11794

Author Contributions

J.H.S., A.P.A., and P.B.S. wrote the paper. J.H.S., P.B.S., R.M.H., G.A.P., and B.E.B. designed the particle bounce research. J.H.S. and S.J.D. performed the bounce measurements. J.H.S. analyzed the data related to the bounce measurements and glass transition temperatures. A.P.A. designed and A.P.A., Z.L., A.L.B., and N.E.O. performed and analyzed the AFM and SEM-EDX measurements of single particle composition and spreading ratios. J.H.S., A.P.A., and R.D.C. setup sampling and inlets for the ELPIs (bounce factors), SMPS, and MOUDI. J.H.S. and R.D.C. operated the SMPS and analyzed the SMPS particle size distributions. R.D.C. collected aerosol particles with the MOUDI. A.T.B., H.W.W., and R.J.G. designed, performed, and analyzed data from the HR-ToF-AMS measurements. A.T.B. performed ISORROPIA modeling. J.C.D. and D.R.G. collected filter samples and analyzed particle composition and molar mass utilizing HPLC-ESI-ToF-MS. J.H.F., S.L.A., M.H.E., R.J.G., and H.W.W. designed, performed, and analyzed data from the measurements of meteorological data and SO_2. All authors contributed intellectually to the manuscript.

Notes

The authors declare no competing financial interest.

■ ACKNOWLEDGMENTS

J.H.S. and P. B. S. acknowledge support from the National Science Foundation (NSF grant CHE-1550398). A.P.A. acknowledges support from the NSF (CAREER award CHE-1654149), University of Michigan M-Cubed program and the University of Michigan Water Center. J.H.S. would like to thank D. A. Knopf, M. Shiraiwa, and A. Laskin for helpful discussions during preparation of this manuscript. A.P.A., Z.L., and A.L.B. acknowledge Prof. M. Banaszak Holl and the Scanning Probe Microscopy (SPM) facility in the University of Michigan, Department of Chemistry for access to the atomic force microscopy instrument. A.P.A and N.E.O. acknowledge the University of Michigan College of Engineering for financial support of the Michigan Center for Materials Characterization (MC^2) for use of the scanning electron microscopy instrument and staff assistance. R.J.G., A.T.B., and H.W.W. acknowledge support from NSF (NSF grant AGS-1552086). The authors gratefully acknowledge the NOAA Air Resources Laboratory (ARL) for the provision of the HYSPLIT transport and dispersion model used in this publication.

■ REFERENCES

(1) Hallquist, M.; Wenger, J. C.; Baltensperger, U.; Rudich, Y.; Simpson, D.; Claeys, M.; Dommen, J.; Donahue, N. M.; George, C.; Goldstein, A. H.; Hamilton, J. F.; Herrmann, H.; Hoffmann, T.; Iinuma, Y.; Jang, M.; Jenkin, M. E.; Jimenez, J. L.; Kiendler-Scharr, A.; Maenhaut, W.; McFiggans, G.; Mentel, T. F.; Monod, A.; Prevot, A. S. H.; Seinfeld, J. H.; Surratt, J. D.; Szmigielski, R.; Wildt, J. The formation, properties and impact of secondary organic aerosol: current and emerging issues. *Atmos. Chem. Phys.* **2009**, *9* (14), 5155−5236.

(2) Shrivastava, M.; Cappa, C. D.; Fan, J. W.; Goldstein, A. H.; Guenther, A. B.; Jimenez, J. L.; Kuang, C.; Laskin, A.; Martin, S. T.; Ng, N. L.; Petaja, T.; Pierce, J. R.; Rasch, P. J.; Roldin, P.; Seinfeld, J. H.; Shilling, J.; Smith, J. N.; Thornton, J. A.; Volkamer, R.; Wang, J.; Worsnop, D. R.; Zaveri, R. A.; Zelenyuk, A.; Zhang, Q. Recent advances in understanding secondary organic aerosol: Implications for global climate forcing. *Rev. Geophys.* **2017**, *55* (2), 509−559.

(3) Tsigaridis, K.; Daskalakis, N.; Kanakidou, M.; Adams, P. J.; Artaxo, P.; Bahadur, R.; Balkanski, Y.; Bauer, S. E.; Bellouin, N.; Benedetti, A.; Bergman, T.; Berntsen, T. K.; Beukes, J. P.; Bian, H.; Carslaw, K. S.; Chin, M.; Curci, G.; Diehl, T.; Easter, R. C.; Ghan, S. J.; Gong, S. L.; Hodzic, A.; Hoyle, C. R.; Iversen, T.; Jathar, S.; Jimenez, J. L.; Kaiser, J. W.; Kirkevag, A.; Koch, D.; Kokkola, H.; Lee, Y. H.; Lin, G.; Liu, X.; Luo, G.; Ma, X.; Mann, G. W.; Mihalopoulos, N.; Morcrette, J. J.; Muller, J. F.; Myhre, G.; Myriokefalitakis, S.; Ng, N. L.; O'Donnell, D.; Penner, J. E.; Pozzoli, L.; Pringle, K. J.; Russell, L. M.; Schulz, M.; Sciare, J.; Seland, O.; Shindell, D. T.; Sillman, S.; Skeie, R. B.; Spracklen, D.; Stavrakou, T.; Steenrod, S. D.; Takemura, T.; Tiitta, P.; Tilmes, S.; Tost, H.; van Noije, T.; van Zyl, P. G.; von Salzen, K.; Yu, F.; Wang, Z.; Wang, Z.; Zaveri, R. A.; Zhang, H.; Zhang, K.; Zhang, Q.; Zhang, X. The AeroCom evaluation and intercomparison of organic aerosol in global models. *Atmos. Chem. Phys.* **2014**, *14* (19), 10845−10895.

(4) Hodzic, A.; Kasibhatla, P. S.; Jo, D. S.; Cappa, C. D.; Jimenez, J. L.; Madronich, S.; Park, R. J. Rethinking the global secondary organic aerosol (SOA) budget: stronger production, faster removal, shorter lifetime. *Atmos. Chem. Phys.* **2016**, *16*, 7917−7941.

(5) Pöschl, U.; Shiraiwa, M. Multiphase chemistry at the atmosphere-biosphere interface influencing climate and public health in the anthropocene. *Chem. Rev.* **2015**, *115*, 4440−4475.

(6) Virtanen, A.; Joutsensaari, J.; Koop, T.; Kannosto, J.; Yli-Pirila, P.; Leskinen, J.; Makela, J. M.; Holopainen, J. K.; Poschl, U.; Kulmala, M.; Worsnop, D. R.; Laaksonen, A. An amorphous solid state of biogenic secondary organic aerosol particles. *Nature* **2010**, *467* (7317), 824−827.

(7) Virtanen, A.; Kannosto, J.; Kuuluvainen, H.; Arffman, A.; Joutsensaari, J.; Saukko, E.; Hao, L.; Yli-Pirila, P.; Tiitta, P.; Holopainen, J. K.; Keskinen, J.; Worsnop, D. R.; Smith, J. N.; Laaksonen, A. Bounce behavior of freshly nucleated biogenic secondary organic aerosol particles. *Atmos. Chem. Phys.* **2011**, *11* (16), 8759−8766.

(8) Koop, T.; Bookhold, J.; Shiraiwa, M.; Pöschl, U. Glass transition and phase state of organic compounds: dependency on molecular properties and implications for secondary organic aerosols in the atmosphere. *Phys. Chem. Chem. Phys.* **2011**, *13* (43), 19238−19255.

(9) Saukko, E.; Lambe, A. T.; Massoli, P.; Koop, T.; Wright, J. P.; Croasdale, D. R.; Pedernera, D. A.; Onasch, T. B.; Laaksonen, A.; Davidovits, P.; Worsnop, D. R.; Virtanen, A. Humidity-dependent phase state of SOA particles from biogenic and anthropogenic precursors. *Atmos. Chem. Phys.* **2012**, *12*, 7517−7529.

(10) Saukko, E.; Kuuluvainen, H.; Virtanen, A. A method to resolve the phase state of aerosol particles. *Atmos. Meas. Tech.* **2012**, *5*, 259−265.

(11) Kidd, C.; Perraud, V.; Wingen, L. M.; Finlayson-Pitts, B. J. Integrating phase and composition of secondary organic aerosol from the ozonolysis of α-pinene. *Proc. Natl. Acad. Sci. U. S. A.* **2014**, *111* (21), 7552−7557.

(12) Pajunoja, A.; Hu, W. W.; Leong, Y. J.; Taylor, N. F.; Miettinen, P.; Palm, B. B.; Mikkonen, S.; Collins, D. R.; Jimenez, J. L.; Virtanen, A. Phase state of ambient aerosol linked with water uptake and chemical aging in the southeastern US. *Atmos. Chem. Phys.* **2016**, *16* (17), 11163−11176.

DOI: 10.1021/acs.est.8b07319
Environ. Sci. Technol. 2019, 53, 4977−4987

(13) Shiraiwa, M.; Li, Y.; Tsimpidi, A. P.; Karydis, V. A.; Berkemeier, T.; Pandis, S. N.; Lelieveld, J.; Koop, T.; Poschl, U. Global distribution of particle phase state in atmospheric secondary organic aerosols. *Nat. Commun.* **2017**, *8*, 15002.
(14) Freedman, M. A. Phase separation in organic aerosol. *Chem. Soc. Rev.* **2017**, *46* (24), 7694−7705.
(15) Reid, J. P.; Bertram, A. K.; Topping, D. O.; Laskin, A.; Martin, S. T.; Petters, M. D.; Pope, F. D.; Rovelli, G. The viscosity of atmospherically relevant organic particles. *Nat. Commun.* **2018**, *9*, 956.
(16) DeRieux, W.-S. W.; Li, Y.; Lin, P.; Laskin, J.; Laskin, A.; Bertram, A. K.; Nizkorodov, S. A.; Shiraiwa, M. Predicting the glass transition temperature and viscosity of secondary organic material using molecular composition. *Atmos. Chem. Phys.* **2018**, *18*, 6331−6351.
(17) Shiraiwa, M.; Ammann, M.; Koop, T.; Pöschl, U. Gas uptake and chemical aging of semisolid organic aerosol particles. *Proc. Natl. Acad. Sci. U. S. A.* **2011**, *108* (27), 11003−11008.
(18) Renbaum-Wolff, L.; Grayson, J. W.; Bateman, A. P.; Kuwata, M.; Sellier, M.; Murray, B. J.; Shilling, J. E.; Martin, S. T.; Bertram, A. K. Viscosity of alpha-pinene secondary organic material and implications for particle growth and reactivity. *Proc. Natl. Acad. Sci. U. S. A.* **2013**, *110* (20), 8014−8019.
(19) Slade, J. H.; Knopf, D. A. Multiphase OH oxidation kinetics of organic aerosol: The role of particle phase state and relative humidity. *Geophys. Res. Lett.* **2014**, *41* (14), 5297−5306.
(20) Berkemeier, T.; Steimer, S. S.; Krieger, U. K.; Peter, T.; Poschl, U.; Ammann, M.; Shiraiwa, M. Ozone uptake on glassy, semi-solid and liquid organic matter and the role of reactive oxygen intermediates in atmospheric aerosol chemistry. *Phys. Chem. Chem. Phys.* **2016**, *18* (18), 12662−12674.
(21) Zelenyuk, A.; Imre, D.; Beranek, J.; Abramson, E.; Wilson, J.; Shrivastava, M. Synergy between secondary organic aerosols and long-range transport of polycyclic aromatic hydrocarbons. *Environ. Sci. Technol.* **2012**, *46* (22), 12459−12466.
(22) Shrivastava, M.; Lou, S. J.; Zelenyuk, A.; Easter, R. C.; Corley, R. A.; Thrall, B. D.; Rasch, P. J.; Fast, J. D.; Simonich, S. L. M.; Shen, H. Z.; Tao, S. Global long-range transport and lung cancer risk from polycyclic aromatic hydrocarbons shielded by coatings of organic aerosol (vol 114, pg 1246, 2017). *Proc. Natl. Acad. Sci. U. S. A.* **2017**, *114* (11), E2263−E2263.
(23) Perraud, V.; Bruns, E. A.; Ezell, M. J.; Johnson, S. N.; Yu, Y.; Alexander, M. L.; Zelenyuk, A.; Imre, D.; Chang, W. L.; Dabdub, D.; Pankow, J. F.; Finlayson-Pitts, B. J. Nonequilibrium atmospheric secondary organic aerosol formation and growth. *Proc. Natl. Acad. Sci. U. S. A.* **2012**, *109*, 2836−2841.
(24) Shiraiwa, M.; Seinfeld, J. H. Equilibration timescale of atmospheric secondary organic aerosol partitioning. *Geophys. Res. Lett.* **2012**, *39*, 54008 DOI: 10.1029/2012GL054008.
(25) Zaveri, R. A.; Easter, R. C.; Shilling, J. E.; Seinfeld, J. H. Modeling kinetic partitioning of secondary organic aerosol and size distribution dynamics: representing effects of volatility, phase state, and particle-phase reaction. *Atmos. Chem. Phys.* **2014**, *14*, 5153−5181.
(26) Price, H. C.; Mattsson, J.; Zhang, Y.; Bertram, A. K.; Davies, J. F.; Grayson, J. W.; Martin, S. T.; O'Sullivan, D.; Reid, J. P.; Rickards, A. M. J.; Murray, B. J. Water diffusion in atmospherically relevant alpha-pinene secondary organic material. *Chem. Sci.* **2015**, *6* (8), 4876−4883.
(27) Hodas, N.; Zuend, A.; Mui, W.; Flagan, R. C.; Seinfeld, J. H. Influence of particle phase state on the hygroscopic behavior of mixed organic-inorganic aerosols. *Atmos. Chem. Phys.* **2015**, *15*, 5027−5045.
(28) Zhang, Y.; Chen, Y.; Lambe, A. T.; Olson, N. E.; Lei, Z.; Craig, R. L.; Zhang, Z.; Gold, A.; Onasch, T. B.; Jayne, J. T.; Worsnop, D. R.; Gaston, C. J.; Thornton, J. A.; Vizuete, W.; Ault, A. P.; Surratt, J. D. Effect of the aerosol-phase state on secondary organic aerosol formation from the reactive uptake of isoprene-derived epoxydiols (IEPOX). *Environ. Sci. Technol. Lett.* **2018**, *5*, 167−174.
(29) Liu, P.; Li, Y. J.; Wang, Y.; Bateman, A. P.; Zhang, Y.; Gong, Z.; Bertram, A. K.; Martin, S. T. Highly viscous states affect the browning of atmospheric organic particulate matter. *ACS Cent. Sci.* **2018**, *4*, 207−215.
(30) Murray, B. J. Inhibition of ice crystallisation in highly viscous aqueous organic acid droplets. *Atmos. Chem. Phys.* **2008**, *8* (17), 5423−5433.
(31) Murray, B. J.; Wilson, T. W.; Dobbie, S.; Cui, Z. Q.; Al-Jumur, S. M. R. K.; Mohler, O.; Schnaiter, M.; Wagner, R.; Benz, S.; Niemand, M.; Saathoff, H.; Ebert, V.; Wagner, S.; Karcher, B. Heterogeneous nucleation of ice particles on glassy aerosols under cirrus conditions. *Nat. Geosci.* **2010**, *3* (4), 233−237.
(32) Berkemeier, T.; Shiraiwa, M.; Poschl, U.; Koop, T. Competition between water uptake and ice nucleation by glassy organic aerosol particles. *Atmos. Chem. Phys.* **2014**, *14*, 12513−12531.
(33) Slade, J. H.; Shiraiwa, M.; Arangio, A. M.; Su, H.; Pöschl, U.; Wang, J.; Knopf, D. A. Cloud droplet activation through oxidation of organic aerosol influenced by temperature and particle phase state. *Geophys. Res. Lett.* **2017**, *44*, 1583.
(34) Bateman, A. P.; Gong, Z.; Liu, P.; Sato, B.; Cirino, G. G.; Zhang, Y.; Artaxo, P.; Bertram, A. K.; Manzi, A. O.; Rizzo, L. V.; Souza, R. A. F.; Zaveri, R. A.; Martin, S. T. Sub-micrometre particulate matter is primarily in liquid form over Amazon rainforest. *Nat. Geosci.* **2016**, *9*, 34−37.
(35) Lee, B. H.; Mohr, C.; Lopez-Hilfiker, F. D.; Lutz, A.; Hallquist, M.; Lee, L.; Romer, P.; Cohen, R. C.; Lyer, S.; Kurten, T.; Hu, W.; Day, D. A.; Campuzano-Jost, P.; Jimenez, J. L.; Xu, L.; Ng, N. L.; Guo, H.; Weber, R. J.; Wilde, R. J.; Brown, S. S.; Koss, A.; de Gouw, J.; Olson, K.; Goldstein, A. H.; Seco, R.; Kim, S.; McAvey, K. M.; Shepson, P. B.; Starn, T. K.; Baumann, K.; Edgerton, E. S.; Liu, J.; Shilling, J. E.; Miller, D. O.; Brune, W.; Schobesberger, S.; D'Ambro, E. L.; Thornton, J. A. Highly functionalized organic nitrates in the southeast United States: contribution to secondary organic aerosol and reactive nitrogen budgets. *Proc. Natl. Acad. Sci. U. S. A.* **2016**, *113* (6), 1516−1521.
(36) Lee, A. K. Y.; Abbatt, J. P. D.; Leaitch, W. R.; Li, S. M.; Sjostedt, S. J.; Wentzell, J. J. B.; Liggio, J.; Macdonald, A. M. Substantial secondary organic aerosol formation in a coniferous forest: observations of both day- and nighttime chemistry. *Atmos. Chem. Phys.* **2016**, *16* (11), 6721−6733.
(37) Draper, D. C.; Farmer, D. K.; Desyaterik, Y.; Fry, J. L. A qualitative comparison of secondary organic aerosol yields and composition from ozonolysis of monoterpenes at varying concentrations of NO_2. *Atmos. Chem. Phys.* **2015**, *15* (21), 12267−12281.
(38) Pajunoja, A.; Lambe, A. T.; Hakala, J.; Rastak, N.; Cummings, M. J.; Brogan, J. F.; Hao, L.; Paramonov, M.; Hong, J.; Prisle, N. L.; Malila, J.; Romakkaniemi, S.; Lehtinen, K. E. J.; Laaksonen, A.; Kulmala, M.; Massoli, P.; Onasch, T. B.; Donahue, N. M.; Riipinen, I.; Davidovits, P.; Worsnop, D. R.; Petaja, T.; Virtanen, A. Adsorptive uptake of water by semisolid secondary organic aerosols. *Geophys. Res. Lett.* **2015**, *42* (8), 3063−3068.
(39) Maenhaut, W.; Chi, X. G.; Wang, W.; Cafmeyer, J.; Yasmeen, F.; Vermeylen, R.; Szmigielska, K.; Janssens, I. A.; Claeys, M. Contribution from Selected Organic Species to PM2.5 Aerosol during a Summer Field Campaign at K-Puszta, Hungary. *Atmosphere* **2017**, *8* (11), 221.
(40) Carroll, M. A.; Shepson, P. B.; Bertman, S. B. Overview of the Program for Research on Oxidants: PHotochemistry, Emissions, and Transport (PROPHET) summer 1998. *J. Geophys. Res.* **2001**, *106*, 24275−24288.
(41) Slade, J. H.; VanReken, T. M.; Mwaniki, G. R.; Bertman, S.; Stirm, B. H.; Shepson, P. B. Aerosol production from the surface of the Great Lakes. *Geophys. Res. Lett.* **2010**, *37* (18), L18807.
(42) VanReken, T. M.; Mwaniki, G. R.; Wallace, H. W.; Pressley, S. N.; Erickson, M. H.; Jobson, B. T.; Lamb, B. K. Influence of air mass origin on aerosol properties at a remote Michigan forest site. *Atmos. Environ.* **2015**, *107*, 35−43.
(43) Jarvinen, A.; Aitomaa, M.; Rostedt, A.; Keskinen, J.; Yli-Ojanpera, J. Calibration of the new electrical low pressure impactor (ELPI plus). *J. Aerosol Sci.* **2014**, *69*, 150−159.

DOI: 10.1021/acs.est.8b07319
Environ. Sci. Technol. 2019, 53, 4977−4987

(44) Jain, S.; Petrucci, G. A. A New Method to Measure Aerosol Particle Bounce Using a Cascade Electrical Low Pressure Impactor. *Aerosol Sci. Technol.* **2015**, *49* (6), 390−399.
(45) van Gulijk, C.; Marijnissen, J. C. M.; Makkee, M.; Moulijn, J. A. Oil-soaked sintered impactors for the ELPI in diesel particulate measurements. *J. Aerosol Sci.* **2003**, *34* (5), 635−640.
(46) Bateman, A. P.; Belassein, H.; Martin, S. T. Impactor apparatus for the study of particle rebound: relative humidity and capillary forces. *Aerosol Sci. Technol.* **2014**, *48*, 42−52.
(47) DeCarlo, P. F.; Kimmel, J. R.; Trimborn, A.; Northway, M. J.; Jayne, J. T.; Aiken, A. C.; Gonin, M.; Fuhrer, K.; Horvath, T.; Docherty, K. S.; Worsnop, D. R.; Jimenez, J. L. Field-deployable, high-resolution, time-of-flight aerosol mass spectrometer. *Anal. Chem.* **2006**, *78* (24), 8281−8289.
(48) Craig, R. L.; Bondy, A. L.; Ault, A. P. Surface Enhanced Raman Spectroscopy Enables Observations of Previously Undetectable Secondary Organic Aerosol Components at the Individual Particle Level. *Anal. Chem.* **2015**, *87* (15), 7510−7514.
(49) Gunsch, M. J.; May, N. W.; Wen, M.; Bottenus, C. L. H.; Gardner, D. J.; VanReken, T. M.; Bertman, S. B.; Hopke, P. K.; Ault, A. P.; Pratt, K. A. Ubiquitous influence of wildfire emissions and secondary organic aerosol on summertime atmospheric aerosol in the forested Great Lakes region. *Atmos. Chem. Phys.* **2018**, *18* (5), 3701−3715.
(50) Gunsch, M. J.; Schmidt, S. A.; Gardner, D. J.; Bondy, A. L.; May, N. M.; Bertman, S. B.; Pratt, K. A.; Ault, A. P. Particle growth in an isoprene-rich forest: influences of urban, wildfire, and biogenic air masses. *Atmos. Environ.* **2018**, *178*, 255−264.
(51) May, N. W.; Gunsch, M. J.; Olson, N. E.; Bondy, A. L.; Kirpes, R. M.; Bertman, S. B.; China, S.; Laskin, A.; Hopke, P. K.; Ault, A. P.; Pratt, K. A. Unexpected Contributions of Sea Spray and Lake Spray Aerosol to Inland Particulate Matter. *Environ. Sci. Technol. Lett.* **2018**, *5* (7), 405−412.
(52) Bateman, A. P.; Walser, M. L.; Desyaterik, Y.; Laskin, J.; Laskin, A.; Nizkorodov, S. A. The effect of solvent on the analysis of secondary organic aerosol using electrospray ionization mass spectrometry. *Environ. Sci. Technol.* **2008**, *42* (19), 7341−7346.
(53) Ault, A. P.; Axson, J. L. Atmospheric Aerosol Chemistry: Spectroscopic and Microscopic Advances. *Anal. Chem.* **2017**, *89* (1), 430−452.
(54) Bondy, A. L.; Kirpes, R. M.; Merzel, R. L.; Pratt, K. A.; Banaszak Holl, M. M.; Ault, A. P. Atomic Force Microscopy-Infrared Spectroscopy of Individual Atmospheric Aerosol Particles: Subdiffraction Limit Vibrational Spectroscopy and Morphological Analysis. *Anal. Chem.* **2017**, *89* (17), 8594−8598.
(55) Cheng, Y. F.; Su, H.; Koop, T.; Mikhailov, E.; Poschl, U. Size dependence of phase transitions in aerosol nanoparticles. *Nat. Commun.* **2015**, *6*, 6923 DOI: 10.1038/ncomms6923.
(56) Veghte, D. P.; Altaf, M. B.; Freedman, M. A. Size Dependence of the Structure of Organic Aerosol. *J. Am. Chem. Soc.* **2013**, *135* (43), 16046−16049.
(57) Fard, M. M.; Krieger, U. K.; Peter, T. Kinetic Limitation to Inorganic Ion Diffusivity and to Coalescence of Inorganic Inclusions in Viscous Liquid-Liquid Phase-Separated Particles. *J. Phys. Chem. A* **2017**, *121* (48), 9284−9296.
(58) You, Y.; Renbaum-Wolff, L.; Carreras-Sospedra, M.; Hanna, S. J.; Hiranuma, N.; Kamal, S.; Smith, M. L.; Zhang, X.; Weber, R. J.; Shilling, J. E.; Dabdub, D.; Martin, S. T.; Bertram, A. K. Images reveal that atmospheric particles can undergo liquid−liquid phase separations. *Proc. Natl. Acad. Sci. U. S. A.* **2012**, *109* (33), 13188−13193.
(59) Bondy, A. L.; Craig, R. L.; Zhang, Z.; Gold, A.; Surratt, J. D.; Ault, A. P. Isoprene-Derived Organosulfates: Vibrational Mode Analysis by Raman Spectroscopy, Acidity-Dependent Spectral Modes, and Observation in Individual Atmospheric Particles. *J. Phys. Chem. A* **2018**, *122* (1), 303−315.
(60) Rolph, G.; Stein, A.; Stunder, B. Real-time Environmental Applications and Display sYstem: READY. *Environ. Modell Softw* **2017**, *95*, 210−228.
(61) Liu, Y. C.; Wu, Z. J.; Wang, Y.; Xiao, Y.; Gu, F. T.; Zheng, J.; Tan, T. Y.; Shang, D. J.; Wu, Y. S.; Zeng, L. M.; Hu, M.; Bateman, A. P.; Martin, S. T. Submicrometer Particles Are in the Liquid State during Heavy Haze Episodes in the Urban Atmosphere of Beijing, China. *Environ. Sci. Technol. Lett.* **2017**, *4* (10), 427−432.
(62) Bateman, A. P.; Gong, Z. H.; Harder, T. H.; de Sa, S. S.; Wang, B. B.; Castillo, P.; China, S.; Liu, Y. J.; O'Brien, R. E.; Palm, B. B.; Shiu, H. W.; Cirino, G. G.; Thalman, R.; Adachi, K.; Alexander, M. L.; Artaxo, P.; Bertram, A. K.; Buseck, P. R.; Gilles, M. K.; Jimenez, J. L.; Laskin, A.; Manzi, A. O.; Sedlacek, A.; Souza, R. A. F.; Wang, J.; Zaveri, R.; Martin, S. T. Anthropogenic influences on the physical state of submicron particulate matter over a tropical forest. *Atmos. Chem. Phys.* **2017**, *17* (3), 1759−1773.
(63) Vaden, T. D.; Imre, D.; Beranek, J.; Shrivastava, M.; Zelenyuk, A. Evaporation kinetics and phase of laboratory and ambient secondary organic aerosol. *Proc. Natl. Acad. Sci. U. S. A.* **2011**, *108* (6), 2190−2195.
(64) Zelenyuk, A.; Imre, D. G.; Wilson, J.; Bell, D. M.; Suski, K. J.; Shrivastava, M.; Beranek, J.; Alexander, M. L.; Kramer, A. L.; Simonich, S. L. M. The effect of gas-phase polycyclic aromatic hydrocarbons on the formation and properties of biogenic secondary organic aerosol particles. *Faraday Discuss.* **2017**, *200*, 143−164.
(65) Kundu, S.; Fisseha, R.; Putnam, A. L.; Rahn, T. A.; Mazzoleni, L. R. High molecular weight SOA formation during limonene ozonolysis: insights from ultrahigh-resolution FT-ICR mass spectrometry characterization. *Atmos. Chem. Phys.* **2012**, *12*, 5523−5536.
(66) Kourtchev, I.; Fuller, S.; Aalto, J.; Ruuskanen, T. M.; McLeod, M. W.; Maenhaut, W.; Jones, R.; Kulmala, M.; Kalberer, M. Molecular composition of Boreal forest aerosol from Hyytiälä, Finland, using ultrahigh resolution mass spectrometry. *Environ. Sci. Technol.* **2013**, *47* (9), 4069−4079.
(67) Surratt, J. D.; Chan, A. W. H.; Eddingsaas, N. C.; Chan, M. N.; Loza, C. L.; Kwan, A. J.; Hersey, S. P.; Flagan, R. C.; Wennberg, P. O.; Seinfeld, J. H. Reactive intermediates revealed in secondary organic aerosol formation from isoprene. *Proc. Natl. Acad. Sci. U. S. A.* **2010**, *107*, 6640−66445.
(68) Tolocka, M. P.; Jang, M.; Ginter, J. M.; Cox, F. J.; Kamens, R. M.; Johnston, M. V. Formation of oligomers in secondary organic aerosol. *Environ. Sci. Technol.* **2004**, *38*, 1428−1434.
(69) Heaton, K. J.; Dreyfus, M. A.; Wang, S.; Johnston, M. V. Oligomers in the early stage of biogenic secondary organic aerosol formation and growth. *Environ. Sci. Technol.* **2007**, *41*, 6129−6136.
(70) Sareen, N.; Carlton, A. G.; Surratt, J. D.; Gold, A.; Lee, B.; Lopez-Hilfiker, F. D.; Mohr, C.; Thornton, J. A.; Zhang, Z.; Lim, Y. B.; Turpin, B. J. Identifying precursors and aqueous organic aerosol formation pathways during the SOAS campaign. *Atmos. Chem. Phys.* **2016**, *16*, 14409−14420.
(71) Kessler, S. H.; Nah, T.; Daumit, K. E.; Smith, J. D.; Leone, S. R.; Kolb, C. E.; Worsnop, D. R.; Wilson, K. R.; Kroll, J. H. OH-initiated heterogeneous aging of highly oxidized organic aerosol. *J. Phys. Chem. A* **2012**, *116* (24), 6358−6365.
(72) Malecha, K. T.; Nizkorodov, S. A. Photodegradation of Secondary Organic Aerosol Particles as a Source of Small, Oxygenated Volatile Organic Compounds. *Environ. Sci. Technol.* **2016**, *50* (18), 9990−9997.
(73) Knopf, D. A.; Mak, J.; Gross, S.; Bertram, A. K. Does atmospheric processing of saturated hydrocarbon surfaces by NO3 lead to volatilization? *Geophys. Res. Lett.* **2006**, *33* (17), 26884 DOI: 10.1029/2006GL026884.
(74) Petters, M. D.; Kreidenweis, S. M. A single parameter representation of hygroscopic growth and cloud condensation nucleus activity. *Atmos. Chem. Phys.* **2007**, *7* (8), 1961−1971.
(75) Petters, M. D.; Kreidenweis, S. M. A single parameter representation of hygroscopic growth and cloud condensation nucleus activity - Part 2: Including solubility. *Atmos. Chem. Phys.* **2008**, *8* (20), 6273−6279.
(76) Song, M.; Liu, P. F.; Hanna, S. J.; Li, Y. J.; Martin, S. T.; Bertram, A. K. Relative humidity-dependent viscosities of isoprene-derived secondary organic material and atmospheric implications for

DOI: 10.1021/acs.est.8b07319
Environ. Sci. Technol. 2019, 53, 4977−4987

isoprene-dominant forests. *Atmos. Chem. Phys.* **2015**, *15* (9), 5145−5159.
(77) Slinn, W. G. N. Predictions for Particle Deposition to Vegetative Canopies. *Atmos. Environ.* **1982**, *16* (7), 1785−1794.
(78) Gough, C. M.; Vogel, C. S.; Schmid, H. P.; Curtis, P. S. Controls on annual forest carbon storage: Lessons from the past and predictions for the future. *BioScience* **2008**, *58* (7), 609−622.
(79) Jain, S.; Fischer, K. B.; Petrucci, G. A. The influence of absolute mass loading of secondary organic aerosols on their phase state. *Atmosphere* **2018**, *9* (4), 131.
(80) Lu, J. W.; Rickards, A. M. J.; Walker, J. S.; Knox, K. J.; Miles, R. E. H.; Reid, J. P.; Signorell, R. Timescales of water transport in viscous aerosol: measurements on sub-micron particles and dependence on conditioning history. *Phys. Chem. Chem. Phys.* **2014**, *16* (21), 9819−9830.
(81) Altaf, M. B.; Freedman, M. A. Effect of Drying Rate on Aerosol Particle Morphology. *J. Phys. Chem. Lett.* **2017**, *8* (15), 3613−3618.

DOI: 10.1021/acs.est.8b07319
Environ. Sci. Technol. 2019, 53, 4977−4987